On this line, the partial differential equation (A8) becomes an ordinary first-order differential equation for $\Sigma_{rt}^{(\infty)}$, if we consider x to be variable and $\hat{G}\Delta$ to be fixed. In terms of the variable x, $\Sigma_{rt}^{(\infty)}$ then satisfies the differential equation (32).

To find $\Sigma_{lf}^{(\infty)}$, we define the generating function

$$\tilde{g}(u,v)=\sum_{l=0}^{\infty} v^l \sum_{r=1}^{\infty} u^r N_{r,l} \tag{A12}$$

and make use of the symmetry relation (26) for $N_{r,l}$ and its exception (24). We obtain

$$\tilde{g}(u,v)=u-v+g(v,u), \tag{A13}$$

from which we obtain equation (35) relating $\Sigma_{lf}^{(\infty)}(x;\hat{G};\Delta)$ to $\Sigma_{rt}^{(\infty)}(1-x;\hat{G};-\Delta)$.

To relate diagrams contributing to Σ_t with those contributing to Σ_{t+1} we note that all single-loop diagrams with $t+1$ pseudofermion lines can be generated from all diagrams with t lines as follows. We have already shown that any diagram yielding a contribution $-\Delta(-x)^r(1-x)^l(\Delta\hat{G})^{r+l-1}$ gives rise to a set of diagrams of one higher order by replacing either a right-going or left-going line with both a right- and left-going line and including an additional electron line. The sum of all such diagrams can be generated by applying the operator $\Delta\hat{G}x(1-x)d/dx$ to the parent diagram. Since each diagram of order $t+1=r+l+1$ can be generated from a unique parent of order t in this way, the sum of all single-loop diagrams of order $t+1$, which we denote by Σ_{t+1} is given by (36).

*Present address: Department of Physics, The American University, Washington, D. C. 20016.

[1]J. S. Langer, J. Math. Phys. **2**, 584 (1961).
[2]F. Yonezawa and T. Matsubara, Prog. Theor. Phys. **35**, 357 (1966).
[3]F. Yonezawa and T. Matsubara, Prog. Theor. Phys. **35**, 759 (1966).
[4]P. L. Leath and B. Goodman, Phys. Rev. **148**, 968 (1966).
[5]P. L. Leath and B. Goodman, Phys. Rev. **175**, 963 (1968).
[6]D. W. Taylor, Phys. Rev. **156**, 1017 (1967).
[7]F. Yonezawa, Prog. Theor. Phys. **40**, 734 (1968).
[8]P. L. Leath, Phys. Rev. **171**, 725 (1968).
[9]L. Schwartz and E. Siggia, Phys. Rev. B **5**, 383 (1972).
[10]R. J. Elliott and D. W. Taylor, Proc. R. Soc. A **296**, 161 (1967).
[11]P. W. Anderson, Phys. Rev. **109**, 1492 (1958).
[12]The generalization to several bands and to perturbations that have *any* matrix elements nonvanishing (rather than only the diagonal element at the site of the perturbation) introduces no fundamental complications in the formalism.
[13]M. Gaudin, Nucl. Phys. **15**, 89 (1960).
[14]The CPA has, of course, also been obtained in other ways by D. W. Taylor (Ref.6), P. Soven [Phys. Rev. **156**, 809 (1967)], Y. Onodera and Y. Toyozawa [J. Phys. Soc. Jap. **24**, 341 (1968)], and B. Velický, S. Kirkpatrick, and H. Ehrenreich [Phys. Rev. 175, 747 (1968)].

PHYSICAL REVIEW B VOLUME 7, NUMBER 12 15 JUNE 1973

Electron-Excited Auger-Electron Spectrum of a Ni(110)-$c(2\times2)$S Surface: Line-Shape Analysis and Correlation with Ion-Neutralization Spectroscopy

E. N. Sickafus
Ford Motor Company, Scientific Research Staff, Dearborn, Michigan 48121
(Received 9 August 1972)

Electron-excited Auger-electron spectra of a Ni(110)-$c(2\times2)$S surface are correlated with the corresponding spectra obtained by ion-neutralization spectroscopy (data of Becker and Hagstrum). It is found that the sulfur $L_{2,3}VV$ line is characterized by a threshold at 159 eV, a width $\sim$30 eV, and major peaks at 146 and 135 eV. The same structural features are found in both types of spectra, but different relative magnitudes of peak structure are observed. However, this difference may result in part from a fundamental assumption regarding the transition density function that was invoked to facilitate the comparison of the two types of spectra. The electron-excited spectroscopy yields information about levels deeper in the band than does the ion-neutralization spectroscopy due to the use of lower-lying core holes which provide relatively more potential energy for the Auger excitation. Calculations of Auger line shape from simple density-of-states models reveal how each pair of peaks in the latter gives rise to three peaks in the corresponding secondary-electron characteristic (Auger line shape) $N(E)$, and how the background can produce a peak in $N(E)$.

I. INTRODUCTION

Detailed analyses, such as line-shape considerations, have constituted only a small percentage of the Auger-electron-spectroscopy (AES) literature.[1] This is an oversight of some consequence with respect to optimizing the use of experimental data for understanding the properties of surfaces. The significance of the Auger line shape, relative to surface characterization, was anticipated in the early

work of Lander.[2] He demonstrated that the density of electron states (DOS) at the surface is inherently convolved into the Auger line shape for transitions involving the valence band. This information has been used effectively by Hagstrum and Becker[3] in the study of the electron environment of surface atoms using ion-neutralization spectroscopy (INS). The significance of line shape has been recognized in some AES studies.[4-7]

It is the purpose in this paper to analyze the fine structure in electron-excited Auger spectra of a Ni(110)-$c(2\times2)$S surface and to demonstrate its correlation with INS data. The analysis is based on the mathematical statement of Auger line shape given by Lander and uses simple DOS models to predict significant characteristics of $N(E)$ and of dN/dE spectra. $N(E)$ is the number of electrons in the secondary emission having energy E. Credibility of the fine-structure analysis is based on a detailed correlation with the INS data of Becker and Hagstrum[8] for the same Ni(110)-$c(2\times2)$S surface structure.

The term fine structure will be used to refer to Auger line shape in a region of the spectrum including energies higher than and lower than a major Auger peak. The extent of this region is taken to be twice the occupied energy width of the electronic band furnishing electrons for the major Auger peak in question. The position of the major Auger peak relative to its associated region of fine structure is an *a posteriori* determination based on the specific character of the DOS.

Identification of peaks within the Auger fine structure has been reported in the literature by techniques based on several points of view. These are summarized in the introduction to Sec. II. In Sec. III are model calculations of the fine structure derived from simple models for the local density of states. Specific details of the model calculations of $N(E)$ and dN/dE line shape from fabricated DOS models are summarized in the Appendix. In Sec. V are presented $N(E)$ and dN/dE line-shape data for the sulfur Auger peak characteristic of the electron-excited Auger spectrum of a Ni(110)-$c(2\times2)$S surface; experimental details are summarized in Sec. IV. The corresponding spectra derived from the INS data of Becker and Hagstrum are compared with those of electron-excited AES in Sec. VI. The paper concludes with summary remarks and observations in Sec. VII.

II. FINE-STRUCTURE IDENTIFICATION

Most peaks in dN/dE spectra of AES can be characterized as having an easily recognized major feature associated with less-pronounced fine structure. Customarily, this major feature is marked on an energy scale and identified with tabulated electron binding energies. We are concerned here with a proper interpretation of the major Auger feature and the identification of the associated fine structure occupying a region which can extend to either side of the major Auger feature. The width of the energy range containing the associated fine structure is sufficient to include effects which have been described in other papers, for other systems, as resulting from certain specified phenomena. These other descriptions are outlined briefly so as to set a proper framework with which to understand the emphasis of this work.

At least four approaches to the identification of Auger fine structure are reported in the literature. In one approach peaks in the region neighboring a major peak are identified via correlation with tabulated binding energies as commonly is done with the major peak. This leads to a triplet notation of atomic levels, one for the core hole and two for the initial states of the two electrons (e.g., KL_1L_1, $L_3M_{2,3}M_{2,3}$, and other core-core-core transitions), with which to characterize each peak. A spectroscopic term is appended [e.g., $WXY\,(^1S_0)$] to designate the final state of the doubly ionized ion in cases where LS coupling plays a more dominant role than jj coupling. This approach has been used, for example, in the case of Auger peaks occurring 16 eV apart for aluminum and within a span of 12 eV for tin,[9] for peaks occurring 9 eV and 11 eV apart for thallium and 20 eV apart for bismuth[10] (β-ray spectrometry), 20 eV apart for manganese[11] (electron-capture decay of ^{55}Fe), and for peaks 10 eV or less apart in spectra of scandium, titanium, vanadium, iron, and cobalt.[12]

A second approach to identification of Auger fine structure is to consider peaks that occur in the near low-energy region of a major Auger peak as resulting from characteristic energy losses experienced by escaping electrons originally identified with the major peak. This has been done, for example, in the case of a 17 eV (plasmon) loss below an 87-eV Si peak,[13,14] for a 14.6-eV (plasmon and interband) loss below the $M_2M_{4,5}M_{4,5}$-$M_3M_{4,5}M_{4,5}$ Cu doublet,[15] and for an 11-eV loss on In associated with the $M_5N_5N_5$ Auger transition (similar results were found for Cd, Ag, Zn, Ti, and C spectra).[14] A deconvolution scheme has been developed for the removal of characteristic loss effects as well as instrument broadening effects. The method has been applied to studies of In, CdS, and oxygen adsorbate structures, and the results compared with electron-spectroscopy-for-chemical-analysis (ESCA) data.[16]

In a third appraoch to Auger-fine-structure identification a characteristic energy gain is attributed to escaping electrons originally belonging to the major Auger transition. These show up in the spectrum in the near high-energy region of the major peak in a fashion analogous to the characteristic

losses previously described. Examples of this type of identification are a gain doublet having a mean energy at 7.5 eV above the mean energy of the $M_2M_{4,5}M_{4,5}$-$M_3M_{4,5}M_{4,5}$ Cu doublet,[15] a gain (plasmon) appearing in an Al spectrum at 82 eV relative to the major peak ($L_{2,3}VV$) occurring at 67 eV,[17] and the 103-eV peak in the silicon spectrum.[18] It has been suggested that an alternative interpretation of "plasmon gains" might be based on Auger transitions involving excited hole states in the ion core.[19]

The interpretation of Auger fine structure by the fourth method emphasizes the inherent role of the band structure of the substrate. Such analyses have been used in studies of graphite single crystals,[4] clean beryllium surfaces,[5] oxidized beryllium surfaces,[6] and the (111) surface of silicon.[7] Reference to this type of interpretation is designated in a general fashion as, for example,[13,20] KVV, LVV, etc., meaning core-band-band transitions. Included here are the so-called "chemical-shift" effects[21-23] although they may not have invoked specific details of the band structure. This rather general designation iVV is in fact an appropriate syllogistic label for Auger peaks that characterize surface atoms, because electronic effects unique to a surface atom, such as surface molecular orbitals, are expected to be more pronounced among the valence-band electrons than the deeper-lying core states.

As a conceptual model of the surface it is convenient to visualize three regions: the bulk, the selvedge, and the vacuum. The selvedge is that region of the surface where physical properties have modified values relative to their bulk values. It is generally considered that the selvedge is distinguished from the bulk by change in atomic arrangement. In particular, the selvedge has one less periodic dimension. The nature of a physical property of the bulk, such as the electron density of states, on passing through the selvedge varies from values characteristic of the bulk to some limiting value at the vacuum-selvedge interface (or other characteristic position relative to the outermost ion-core potential wells). In the case of a fractional monolayer of a different atomic species being introduced at the surface of an otherwise atomically clean substrate a new selvedge results.

It is assumed that the local density of states at an atom (any species) in the selvedge is obtained from the bulk density of states by weighting the density of states for the bulk by the square of the wave function at the local atom and then integrating over the region of the local atom. The formation of a new selvedge by the addition of a new atomic species may be accompanied by changes in the local density of states in the selvedge. Molecular orbitals associated with bonding of the new atomic species can cause enhancement of the local wave function with consequential changes in the local density of states.[3(a)]

In this paper interest is placed on correlating Auger fine structure of iVV transitions with the valence-band density of states and resonance effects associated with surface molecular orbitals. Two guiding principles are invoked in this analysis. First, the kinetic energies of the observed Auger electrons are related to core-level energies, the occupied width of the valence band, and the work function of the surface. Second, the population distribution in the observed Auger line shape is related to band structure and associated resonance effects via a convolution integral.

The kinetic energies of Auger electrons are determined by three different electron energy levels. Electron bombardment of a surface of a condensed phase generates Auger transitions by ionization of a core level i leaving a hole that is filled by a "down electron" from the level j and an accompanying energy dissipation via ejection of an "up electron" from the level k. The kinetic energy relative to the vacuum level E_{ijk} of the up electron is determined by the binding energies of the electron levels i,j, and k according to

$$E_{ijk} = E_i(Z) - E_j(Z) - E_k(Z+1)\,, \tag{1}$$

where Z is the atomic number. The $(Z+1)$ of the last term suggests an approximation to the appropriate binding energy. The role of the condensed phase comes into play by providing a continuum of band states for the j and k levels in iVV-type transitions. Structure in the Auger line shape derives from the fact that the observed electron population with kinetic energy E_{ijk} reflects differing transition densities associated with different levels j and k. The range of this structure around a given Auger peak is twice the occupied width of the band and can amount to an energy region ~25-eV wide [in $N(E)$ and dN/dE spectra]. The energy-doubling effect in the relationship between the occupied bandwidth and the width of the Auger line is illustrated in Figs. 1 and 2.

The role of the band structure in determining the Auger line shape is given by the convolution product of the density of states $N(\zeta)$, shown originally by Lander,[2] as

$$\tilde{N}(\zeta) = N(\zeta) * N(\zeta) \equiv \int_0^{\zeta} N(\zeta-\Delta)N(\zeta+\Delta)d\Delta$$

for

$$0 \le \zeta \le \zeta_b/2,$$

and (2)

$$\tilde{N}(\zeta) \equiv \int_0^{\zeta_b-\zeta} N(\zeta-\Delta)N(\zeta+\Delta)d\Delta$$

for

$$\zeta_b/2 \le \zeta \le \zeta_b\,,$$

where ζ is the mean energy of the j and k states within the band measured relative to the Fermi level. The first integral covers the range of the convolution variable Δ in the upper half of the band while the second integral completes the range of Δ to the bottom of the band ζ_b; see Fig. 1. A type of redundancy is inherent in the convolution product $\tilde{N}(\zeta)$ in that one of the functions in each of the integrands of Eq. (2) extends into the range of the other integral for certain values of ζ; for example, $N(\zeta+\Delta)$ in the first integral extends into the range of the second integral when $\zeta_b/4 < \zeta < \zeta_b/2$. This convolution product is proportional to the internal excited-electron distribution $F_c(E)$, where

$$E = |E_i| - 2(\zeta + \varphi) \tag{3}$$

and φ is the work function, provided that certain simplifying assumptions are valid.[24] These assumptions are that the transition probability is independent of band energy ζ, initial-state k vector, symmetry character of the band, and possible many-body effects as well as final-state interactions. The relation between $F_c(E)$ and the experimentally observed Auger line shape depends upon the escape probability of the electrons $P(E)$ (see Fig. 2), an instrument function characterizing the sensitivity and resolution of the detector, and scattering phenomena during escape (e.g., characteristic energy losses). Superposing structure from neighboring (independent) spectral features may add further complications to the observed line

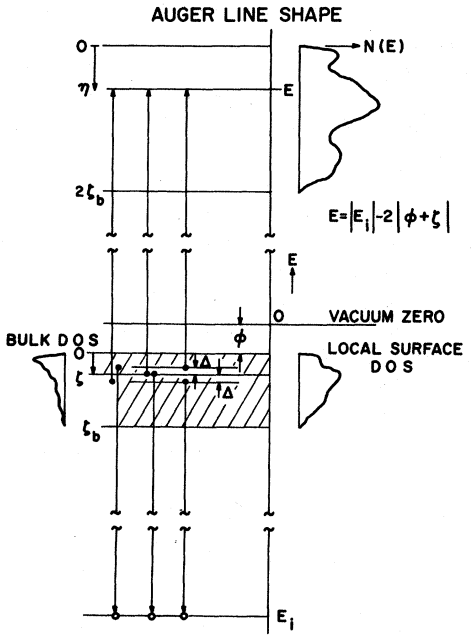

FIG. 1. Energy-level diagram showing the correspondence between the local density of states DOS and the Auger line shape $N(E)$.

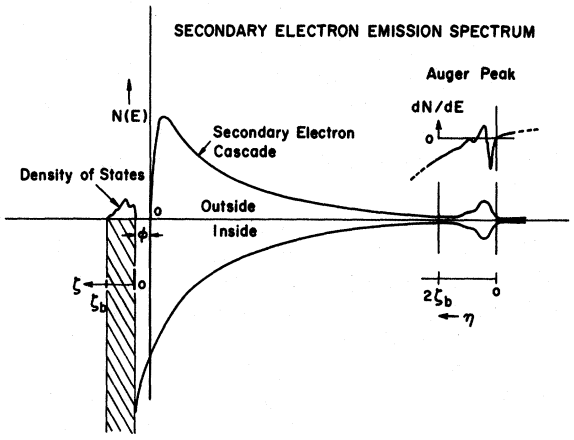

FIG. 2. Secondary-emission spectrum showing the relationship between the band structure and the emitted Auger spectrum along with its attendant background due to the secondary-electron cascade. The difference between the inside and outside secondary-electron distributions, shown mirrored in the abscissa, is due to the effect of escape probability.

shape. Surface specificity of the resulting Auger-line-shape information is governed by how the escape depth of the Auger electrons compares with the depth to which the surface density of states is different from the bulk density of states.

Hagstrum and Becker[24] have used a deconvolution procedure governed by Eq. (2) to unfold INS data so as to reveal what they term a transition density $U(\zeta)$. This is essentially the density of states $N(\zeta)$ if the stated simplifying assumptions are valid. They have applied their analysis to the INS spectrum of a Ni(110)-$c(2\times2)$S surface and their results will be incorporated in this paper in a later section.

Electron-excited Auger-electron spectra (EEAES) and ion-neutralization spectra have the same fundamental dependence on the convolution product of the DOS as given in Eq. (2). They differ, however, in the following manner: (i) In INS the electronic character of the surface region is probed by the tunneling of a band electron to the probing ion (e.g., He^+). The probing ion is a third body which does not play a role in EEAES. (ii) The kinetic energy of the incident ion contributes to a physical broadening of the Auger process not present in EEAES. (iii) The ionization energy of the probing gas limits the depth to which the band can be examined; namely, ζ_{max} is one-half the ionization energy minus the work function. This is, however, reasonably deep being of the order of 10 eV below the vacuum level. In EEAES the potential exists to examine the full extent of the band by concentrating on Auger transitions to deep core states. This potential raises another distinction based on the escape depth of the

Auger electrons: (iv) Different Auger transitions in EEAES and the characteristic Auger transition of INS may reveal different apparent state densities because of differing energy dependence of the escape depth. For example, EEAES can detect the local DOS at ion cores buried in the selvedge (and perhaps the bulk) when sufficient energy is provided to the Auger electrons to permit their escape from the solid. (v) The matrix elements describing the transition probabilities may incorporate different contributions from the same electron wave function due to relative differences in atomic location of the Auger events. In EEAES it is the position of the adsorbate-ion core that determines the significant part of the wave function while in INS it is the (variable) position of the probing-ion core that is the determining factor. The latter is more remote from the surface than is the former.

The above discussion has demonstrated that a variety of cause and effect relationships have been invoked to understand Auger line shapes. In principle, it is to be expected that core-core-core transitions should yield less complex Auger line shapes, by comparison, than core-band-band transitions. However, the latter lead to line shapes having explicit information about the electronic modifications of a surface (and atoms) that accompany accommodation of a surface atom. It is this information about the electronic character of a surface that is desired and therefore a proper consideration of line-shape characteristics is needed. We will first examine model calculations in order to identify simple characteristics.

III. MODEL CALCULATIONS

Before attempting to identify fine-structure features in a particular segment of an Auger-electron spectrum it will be useful to consider some general properties of the convolution square of elementary functions. Thus from simple models for DOS functions it can be seen how peaks arise in $N(E)$ and dN/dE curves, how many peaks are to be expected, and whether the peaks in the dN/dE curves are related directly to peaks in the DOS, to the background in the DOS, or to both.

A peaked function u will be constructed from a nonpeaked background b (background in this context refers to a slowly varying, unstructured contribution to u) and a series of independent peaks p_i according to

$$u = b + \sum_i p_i \ . \tag{4}$$

The convolution square of Eq. (4) $u*u$, and its derivative $u'*u$ [note that $u'*u = (u*u)'$] will be examined for various cases where b is zero, a constant, and a linear function, and where the p_i are normalized Gaussian functions. Hagstrum and Becker[24] have discussed the case of $b = 1$ with one Gaussian-like peak and have related the analysis to the problem of unfolding INS data to obtain an appropriate transition density function. Here the scope of the analysis has been extended and DOS functions have been modeled with two Gaussian peaks, a variable background, and a finite (occupied) bandwidth, to show how new peaks arise in the $N(E)$ curve and how their structure may dominate in dN/dE curves.

The convolution square of Eq. (4) has the form shown in Eq. (5):

$$u*u = b*b + 2b*\sum_i p_i + \sum_{i,j} p_i * p_j \ . \tag{5}$$

Its properties for normalized Gaussian peaks can be summarized as follows [in all cases $u(\zeta) \equiv 0$ if $\zeta < 0$ or $\zeta > \zeta_b$]:

A. $b = 0$ (no background): (i) The first two terms of Eq. (5) vanish. (ii) n Gaussian peaks p_i in u yield $n(n+1)/2$ Gaussian peaks in $u*u$ via the third term of Eq. (5). (iii) If p_i has width w_i then $p_i * p_i$ will have width $w_{ii} = \sqrt{2}\, w_i$. In general $w_{ij} = (w_i^2 + w_j^2)^{1/2}$. If p_i and p_j have centroids x_i and x_j, respectively, $p_i * p_j$ has its centroid at the arithmetic mean $(x_i + x_j)/2$. (v) There are $n(n-1)/2$ peaks situated at the arithmetic mean of each pair of peaks in a set n. Hence each pair of peaks in the band produces a new peak in the $N(E)$ spectrum. (vi) The maximum value of $p_i * p_j$ is the product of their individual areas, $A_i A_j$. (vii) The double summation $\sum_{ij}$ produces a term $2p_i * p_j$ (for $i \neq j$) in $u*u$. This yields a peak that can be twice as large as $p_i * p_i$ or $p_j * p_j$, in cases where the area under p_i approaches that under p_j .

B. $b = b$ (constant background): (i) $b*b$ is an isosceles triangle. Thus, the first term of Eq. (5) contributes a peak to $u*u$. (ii) The maximum value of $b*b$ is b^2. (iii) $2b*p_i$ is a Gaussian step centered at the centroid of p_i. The step height asymptotically approaches $2bA_i$, where A_i is the area of p_i.

C. $b = b\zeta$ (linear background): (i) $b*b$ is a cubic term that produces a well-defined peak. (ii) The maximum value of $b*b$ is $\frac{2}{3}(\sqrt{2}-1)b^2\zeta_b^3$, where ζ_b is the width of the band. (iii) The peak of $b*b$ occurs at $\zeta_b/\sqrt{2}$. (iv) $2b*p_i$ is the sum of three terms: a constant plus a Gaussian, whose width is equal to that of p_i and whose centroid in the $N(E)$ spectrum is equal to the centroid of p_i in the band, plus a Gaussian step multiplied by a linear term.

Most of the features described are illustrated in the model calculation shown in Figs. 3–6. The calculations are summarized in the Appendix.

In Figs. 3–6 two sets of three graphs are shown. The left most graph of a set represents u (the model DOS) displayed on an arbitrary energy scale having ten equal units increasing in order from the Fermi level at the right-hand end of the scale (marked 0). The center graph is the corresponding

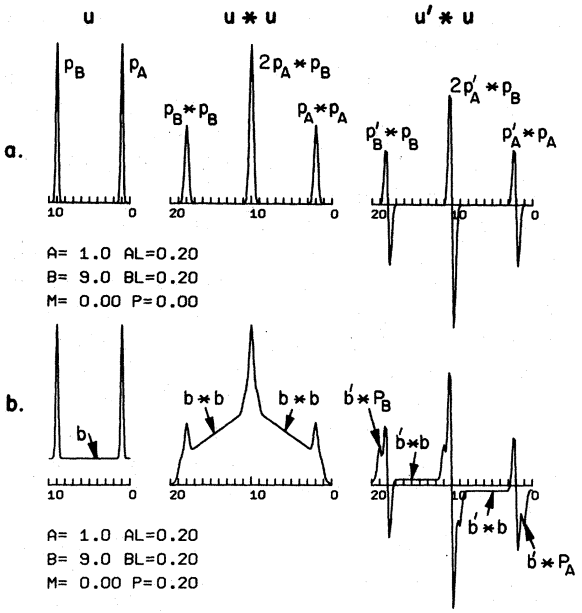

FIG. 3. Model calculations of u, $u*u$, and $u'*u$, for a two-peak density-of-states function. (a) Two Gaussian peaks of equal height and width without a background. (b) The same two Gaussians as in (a) with a constant background of ~17% of a Gaussian peak height.

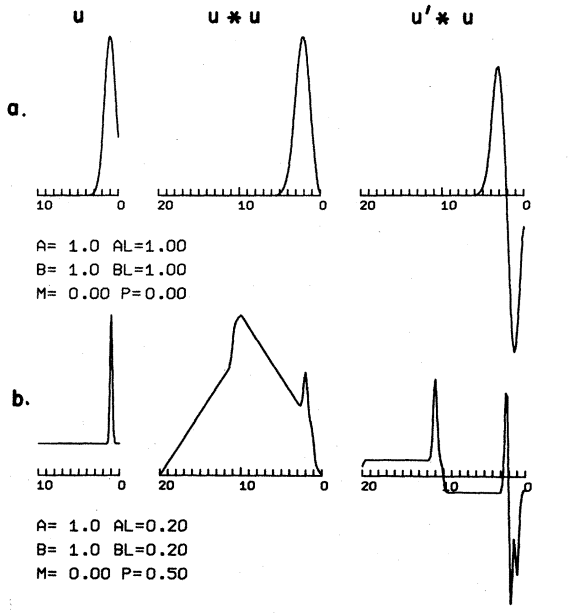

FIG. 5. Model calculation of u, $u*u$, and $u'*u$, for a single-peak density-of-states function. (a) One Gaussian peak with no background but positioned so close to the threshold as to be truncated. (b) A narrow Gaussian peak having the same location as in (a) and with a constant background.

$u*u$ curve, the model $N(E)$ calculated from Eq. (2). It has twenty equal energy units as a result of the energy-doubling effect of the two-electron Auger transition. The right most graph is $u'*u$ (the model energy derivative dN/dE) corresponding to the center graph. The parameters used in the calculations are A, the centroid of a normalized Gaussian of width $AL/\sqrt{2}$, B and BL, analogous values of a second normalized Gaussian, M, the slope of the background, and P, its intercept at 10 on the abscissa.

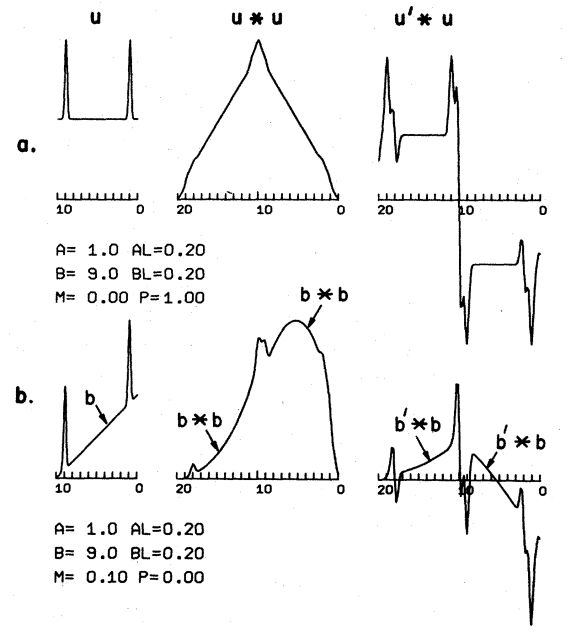

FIG. 4. Model calculations of u, $u*u$, and $u'*u$, for a two-peak density-of-states function. (a) The same two Gaussian as in Fig. 3(a) with a constant background of ~50% of a Gaussian peak height. (b) The two Gaussian peaks of (a) with a linear background.

In Fig. 3(a) two equal Gaussians are positioned at 1 and 9 with no background. Their individual convolution squares appear at 2 and 18 in $u*u$ and $u'*u$ along with their convolution product at 10 [see paragraph A(iv)]. For the case of two equal Gaussians their convolution product is a larger peak in the spectrum than is either of their convolution squares [A(vii)]. It should be noted that in this idealized situation of sharp energy levels within the DOS the resulting $N(E)$ spectral lines have a clear interpretation. The lines that result from the convolution square of a sharp energy level in the DOS represent possible Auger transitions in which both the down and up electrons originate in this energy level. The line resulting from the convolution product of two sharp levels would represent transitions in which one of the two electrons (either one) originated in one level and the second electron originated in the other level.

In Figs. 3(b), 4(a), and 4(b) the effects of adding a background to the model DOS are illustrated: A

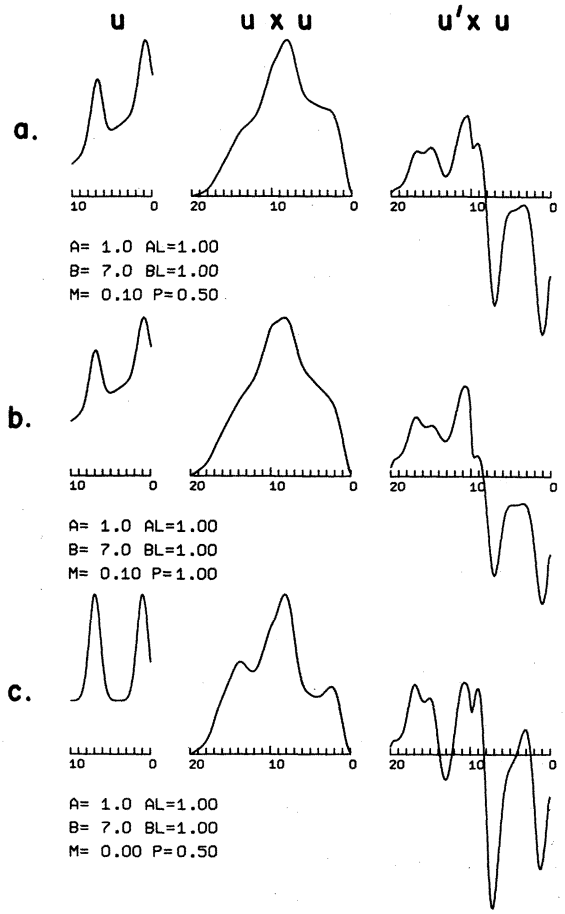

FIG. 6. Model calculations of u, $u*u$, and $u'*u$ for a two-peak density-of-states function consisting of two broad Gaussian peaks one of which is truncated at the threshold of u: (a) linear background, (b) linear background larger than in (a) having the same slope but larger intercept, and (c) constant background having the same intercept as in (a) but different slope.

constant [3(b), 4(a)] and linear [4(b)] background are considered. Recall that, as shown by Eqs. (4) and (5), if u is composed of multiple terms then structural features of the spectrum ($u*u$) arise by summation of the convolution of the various terms. Hence the features of Fig. 3(a) are evidenced in 3(b), 4(a), and 4(b). It can be seen that a constant background in u produces a broad triangular peak in the corresponding spectrum $u*u$. A linear background in u generates a cubic background in $u*u$ and has a corresponding peak that is relatively narrow. Thus we see that peaks can arise in the spectrum $u*u$ that are not due to maxima in the DOS but are due to the nature of the Auger transform (a consequence of the available phase space). Furthermore, these peaks obviously have no simple interpretation regarding assignment of energy levels to Auger transitions. At each energy value 2ζ within the spectrum all accessible levels ζ within the band are mixed by the down and up transitions according to Eq. (2).

Although the background peak is the dominant feature in the spectrum of Fig. 4(b) it is not so pronounced in the corresponding derivative spectrum (shown to the right). However, if the narrow-line features were "washed out" (e.g., by poor instrument resolution) only the background would remain and would be characterized by an asymmetric negative maximum in dN/dE. If such spectra were detected experimentally with an analyzer of finite resolution relatively narrow features might not be resolved and the characteristics of the observed spectrum might only relate to DOS background information. The general asymmetry of the background in $u'*u$ of Fig. 4(b) is somewhat analogous to the characteristic asymmetry of a typical carbon peak in the AES.

The u function of Figs. 3(b), 4(a), and 4(b) have in common nonvanishing backgrounds. As a result of the finite backgrounds their corresponding $u'*u$ curves have a similar negative peak near 1 (and positive peak near 9) on their energy scales. These peaks result from the convolution product of the constant background with a Gaussian peak as labeled in Fig. 3. If the Gaussian has its centroid at $\zeta = a$ in u and b is a constant then their convolution product will have its maximum at $\eta = a$ in $u'*u$.

In Fig. 5 a single-peak u function is illustrated with and without a background and having two different Gaussian peak widths. The wider peak is shown in Fig. 5(a) with no background but positioned so close to the band threshold that the function becomes truncated. This results in a slightly truncated Gaussian in $u*u$ and a truncated Gaussian derivative in $u'*u$. When the peak is made more narrow so as not to become truncated at the band edge and a background is added [see Fig. 5(b)] then both the derivative of the peak and the derivative of the peak-background convolution product are apparent in $u'*u$.

Some effects associated with changes in background structure are illustrated in Fig. 6. Two fixed Gaussian peaks are shown in Figs. 6(a), 6(b), and 6(c) superimposed on backgrounds having the same slopes but different intercepts [6(a) and 6(b)] and having the same intercepts but different slopes [6(a) and 6(c)]. The total amount of background (i.e., the area under b) is least in 6(c) and increases in 6(a) and 6(b), in that order. The first increase in total background [6(c)–6(a)] reduces the relative magnitude of the prominent central peak in $u'*u$. Additional decrease in resolution (relative peak-to-valley separation) is seen between 6(a) and 6(b).

IV. EXPERIMENTAL TECHNIQUE

Details of specimen preparation have been published earlier[25] and are only briefly summarized

here. A single crystal of high-purity nickel was mounted in an ultrahigh vacuum system (UHV) with a (110) surface positioned at the center of a four-grid, low-energy-electron-diffraction (LEED) system. The specimen was heated indirectly by conduction from a tantalum foil to which it was loosely clamped and which was, in turn, heated directly with a dc current. Surface cleaning was done *in situ* by alternate heating and argon-ion-bombardment treatments. The desired sulfur adlayer structure was obtained by annealing the specimen at temperatures in excess of 550 °C which caused surface segregation of sulfur.

Evaluation of the surface condition at various stages of its preparation was done using LEED, EEAES, and secondary-electron-cascade analyses.[26] All of these studies were performed using the same spherical-grid retarding-potential analyzer. In a similar UHV system a second Ni(110) specimen was examined under the same surface conditions.[27] Both systems used spherical-grid (four-grid) retarding-potential analyzers but had different analyzer apertures. The former had an aperture subtending 90° while that of the latter was 120°. Studies in the second system emphasized characteristic electron-energy-loss measurements. Auger line shapes in spectra obtained from these two systems display the same features.

AES data obtained in the first system involved both $N(E)$ and dN/dE spectra of the sulfur Auger peak. These spectra were obtained without the presence of a secondary-electron-cascade background. The background was removed at the signal source by application of an appropriate analog signal designed for this purpose.[26] The $N(E)$ and dN/dE data, without background, are shown in Figs. 7 and 10 (solid-line curves in Fig. 10). The $N(E)$ data were obtained using 2.4-V p-p (Fig. 7) and 0.5-V p-p modulation (Fig. 10) while the dN/dE data were obtained using 3.6-V p-p modulation. In both cases an off-axis electron gun was used to produce a 3-keV primary beam at an incident angle of ~75° with respect to the surface normal. The beam current was 5 μA while the specimen current was 3 μA. All spectra were taken with the specimen maintained at a constant temperature of 300 °C. Specimen temperature was controlled with a closed-loop analog control circuit that derived its error signal from a thermocouple inserted in a small hole in the specimen.

V. SULFUR AUGER LINE SHAPE

The Auger-electron spectrum spanning the energy range of 80–180 eV for a Ni(110)-$c(2\times2)$S selvedge is shown in Fig. 7. Both the $N(E)$ and dN/dE spectra are shown.

The $N(E)$ spectrum shows three well-defined peaks: a major peak at 146 eV, a well-defined peak at 100 eV, and a small peak at 135 eV, on the low-energy tail of the major peak. The first two peaks are identified as follows. Tabulated binding energies[28] relative to the Fermi level—^{16}S: $L_{2,3}$, 164.8±0.7 eV; ^{28}Ni: M_1, 111.8±0.6 eV, $M_{2,3}$, 68.1±0.4 eV, $M_{4,5}$, 3.6±0.4 eV—are combined with work function values[8]

$$\varphi(\text{Ni(110)-clean}) = 4.7 \text{ eV},$$

$$\varphi(\text{Ni(110)-}c(2\times2)\text{S}) = 5.3 \text{ eV}$$

to obtain threshold values for the Auger lines in $L_{2,3}VV$ and M_1VV transitions according to Eq. (3):

S, $E(L_{2,3}VV) = 159.5$ eV;

Ni, $E(M_1VV) = 106.5$ eV.

Before comparing these values with the data it should be noted that the energy scale in Fig. 7 (and Fig. 10) has not been corrected for the contact po-

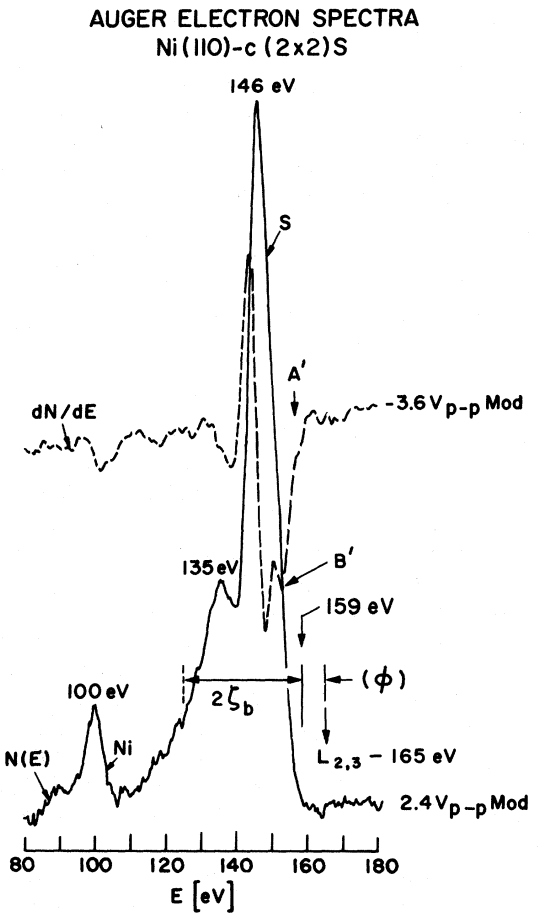

FIG. 7. Electron-excited Auger-electron spectra of a Ni(110)-$c(2\times2)$S surface. The secondary-electron cascade background has been removed at the signal source. The dN/dE spectrum was made at a different modulation amplitude than was the $N(E)$ spectrum. Binding energies are given relative to the Fermi level (see Ref. 28).

tential between the specimen and the retarding grid. This could amount to an error of the order of 1 V (e.g., $\varphi_{\text{grid}} - \varphi_{\text{specimen}} \approx 4.5 - 5.3 = -0.8$ V), with the recorded energy values being shown as too large by this magnitude. The work function of the retarding-potential grid (tungsten mesh) was not measured and therefore the contact potential is not known.

As shown in Fig. 7, the observed threshold for the sulfur Auger line is 159 eV, which is within the experimental error of the calculated value of 159.5 eV for an $L_{2,3}VV$ transition. From this threshold the sulfur Auger line should extend $2\zeta_b$ to lower energies. Since the band is at least 11 eV wide (Fig. 8) the peak at 135 eV is taken to be a part of the Auger line shape associated with the $L_{2,3}VV$ transition. The data shown in Fig. 7 in fact are evidence that the band is broader than 11 eV and may be more nearly ~15 eV in width. A bandwidth of this magnitude for nickel is also suggested from theoretical considerations.[29]

The peak shown at 100 eV in Fig. 7 has an observed threshold of 106 eV which compares with the calculated value of 106.5 eV. This peak is due to an M_1VV transition. Note the systematic error of ~1 eV in the observed and calculated threshold values for the S peak and the Ni peak. The threshold is a useful reference for distinguishing iVV Auger peaks.

The line shape of the 100-eV peak suggests that the 100-eV peak may be governed by transition density functions similar to the 146-eV peak. Note the similarity between the low-energy tail of the 100-eV peak and that of the 146-eV peak. Both peaks have a low-energy peak lying at 11-eV lower energy and having approximately one third the principal peak height. Compare the peak at 89 eV with the 100-eV peak and the peak at 135 eV with the 146-eV peak.

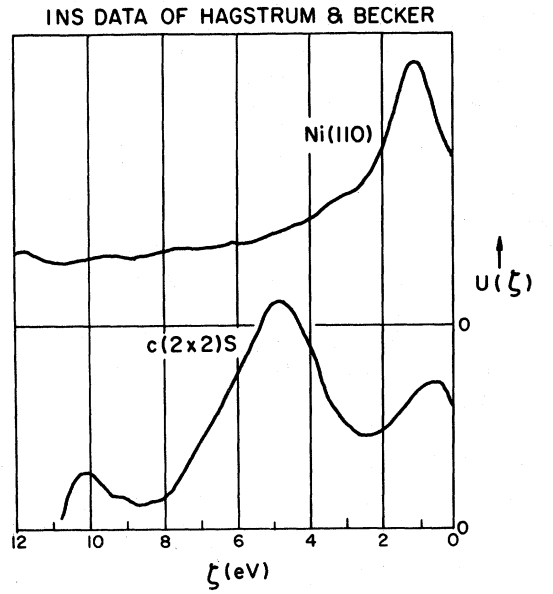

FIG. 8. Unfold function $U(\zeta)$ from ion-neutralization data for a Ni(110) and Ni(110)-$c(2\times 2)$S surface: (a) clean Ni(110) surface, (b) sulfur adlayer in the $c(2\times 2)$ structure. (These curves are presented here through the courtesy of Dr. Becker and Dr. Hagstrum).

The dN/dE data in Fig. 7 show a major peak which is typically identified as the sulfur Auger peak in the more common AES analyses. The maximum excursion of the negative-going part of this peak is the customary point for marking the characteristic energy. It is seen that two additional features are apparent in the dN/dE curve both of which lie to the high-energy side of the negative maximum. They are labeled A' at 157 eV and B' at 154 eV. On comparison with the $N(E)$ data it is clear that they belong with the fine structure of the $N(E)$ sulfur Auger peak. It will be shown that they can be correlated with structure in the transition density function.

The 135-eV peak in $N(E)$ is 11 eV lower in energy than the predominant peak at 146 eV. A characteristic energy loss of 11 eV has been reported for a Ni(110)-$c(2\times 2)$S surface.[30] However, this characteristic loss is not detectable in $N(E)$ loss spectra[27] and requires the advantage of dN/dE spectroscopy to be made evident. It is one of several characteristic losses occurring in the range 5–15 eV below the elastic peak.[27] The peak height of all of these characteristic losses would together only total a few percent of the elastic peak. Whereas, the 135-eV peak seen in Fig. 7 is 32% as large as the 146-eV peak. Consequently, the 135-eV peak is not interpreted to be a characteristic energy-loss peak associated with the 146-eV peak. As will be seen in the Sec. VI, it is a natural consequence of the properties of the DOS and the line-shape convolution.

The width of the sulfur $L_{2,3}VV$ peak in $N(E)$ and the extended low-energy tail may be due in part to instrument broadening resulting from the modulation amplitude. The $N(E)$ spectrum in Fig. 7 was obtained with 2.4-V p-p modulation. This curve can be compared with one taken at lower modulation, 0.5-V p-p, as shown in Fig. 10. The latter curve reveals a narrower peak at 146 eV as well as a high-energy shoulder whose derivative shows up clearly in the dN/dE spectra (labeled B').

VI. CORRELATION OF EEAES AND INS DATA

It is important to note that in this section a fundamental assumption is made regarding the $U(\zeta)$ function from INS. In the previous sections of this paper the discussion is based, *a priori*, on a conceptional view of an occupied density of states of finite width. From this, one constructs convolution integrals, as shown in Eq. (2), having explicit

limits which reflect the characteristic width parameters of the (occupied) DOS. However, a different point of view is used when considering the $U(\zeta)$ data of INS and its comparison with the EEAES data. A $U(\zeta)$ function was derived by Becker and Hagstrum from their $F(\zeta)$ data using the first integral of Eq. (2). In the process of digital-sequential unfolding the starting point corresponds to the Fermi level but the end point is unidentified, lying somewhere within the band not at the band limit ζ_b. The region lying between the terminal point of $U(\zeta)$ and ζ_b is not available from INS data. In lieu of this information, a fundamental assumption is made herein prior to folding $U(\zeta)$ for the purpose of comparison with EEAES data; namely, $U(\zeta)=0$ for ζ greater than the terminal point of the INS $U(\zeta)$, i.e., ζ_m. Using this truncation assumption it becomes possible to calculate an approximation to $F(\zeta)$ in the region $\zeta_m/2 \leq \zeta \leq \zeta_m$ from Eq. (2) as a result of the inherent redundancy that characterizes convolution integrals such as those of Eq. (2). The consequences of this assumption will be pointed out in the ensuing discussion.

The transition-probability-density spectra $U(\zeta)$ deduced from INS data for Ni(110)-clean and Ni(110)-$c(2\times2)$S surfaces are shown in Fig. 8. These spectra are the result of unfolding INS data which have been corrected for kinetic-energy-broadening effects and escape-probability effects.[8] The $U(\zeta)$ curves for a clean Ni(110) surface are characterized by a predominant d band peaked at 1 eV below the Fermi level, as shown in the upper curve of Fig. 8. When sulfur is adsorbed in a $c(2\times2)$S structure the $U(\zeta)$ spectrum acquires two resonance peaks indicative of molecular-orbital structure. A large peak appears near 5 eV and a small peak near 10 eV below the Fermi level, while the residual d band appears to be broadened and shifted to a peak near 0.5 eV below the Fermi level (lower curve in Fig. 8).

In order to compare these $U(\zeta)$ INS data with electron-excited AES data they were convolved and differentiated in accordance with Eq. (2) and the truncation assumption just described. They were not corrected for escape-probability effects, because these effects are constant in the energy region of the sulfur Auger peak, and kinetic-energy broadening does not enter into consideration. The results are shown in Fig. 9. They can be compared with the sulfur $L_{2,3}VV$ AES curves of Fig. 7, $U*U$ with $N(E)$ and $U'*U$ with dN/dE. Both sets of curves have well-defined peaks and corresponding curves appear to have similar structure. The dashed-line portion of the $U*U$ curve, $11<\eta<22$ eV, represents results of these calculations not displayed in the original $F(\zeta)$ curve of Becker and Hagstrum.

A detailed comparison of the two sets of curves is difficult until they are superimposed on the same

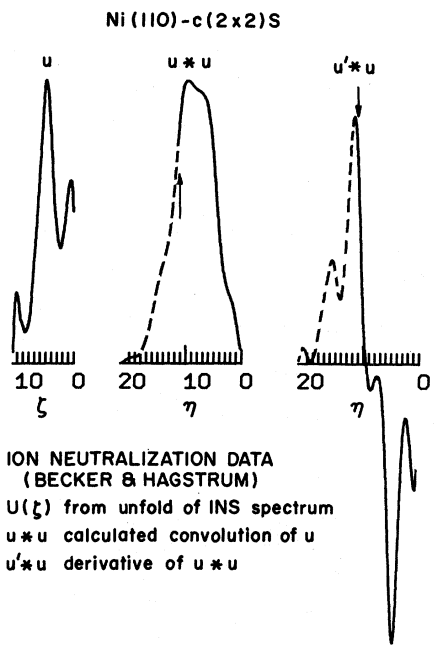

FIG. 9. $U*U$ and $U'*U$ curves calculated from U, as shown in Fig. 8, of ion-neutralization spectroscopy data for a Ni(110)-$c(2\times2)$S spectrum. The dashed-line portions of the curves are regions not displayed in the original $F(\zeta)$ data (see text).

energy scales. This has been done in Fig. 10 where the zero of energy on the $U*U$ and $U'*U$ curves has been placed at 159 eV (the Auger-line-shape threshold).

The agreement between the $N(E)$ and the $U*U$ curves is obvious: Compare the peaks E to e and the peaks at c as well as the overlap of the thresholds and general conformity of line shape. A slight displacement of peak heights at c was introduced to permit comparison of the peak shape. This displacement tends to exaggerate the misfit of the curves in the region b-B.

Agreement of dN/dE and $U'*U$ curves is less striking. However, this is not surprising in view of the use of differentiation of spectra to bring out subtle differences. Consequently, larger differences become increasingly exaggerated. Note the distinct difference in the relative magnitudes of B' with respect to C' and of b' with respect to c'. Without superimposing the spectra it would be easy to confuse C' of dN/dE with b' of $U'*U$. This effect points out a weakness in the practice of assigning characteristic energy values to the position of the most negative excursion of dN/dE. As already shown a better choice of reference might be the threshold of the Auger line.

In view of the above correlation of structural features in $N(E)$ and $U*U$ it is believed that both curves are the result of similar DOS functions.

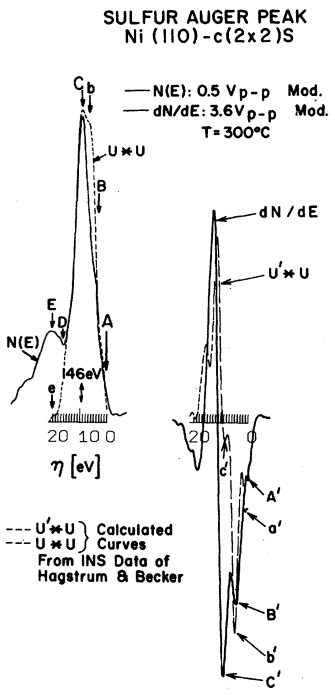

FIG. 10. Comparison of $N(E)$ with $U*U$ and dN/dE with $U'*U$ curves of Figs. 7 and 9. The $N(E)$ and $U*U$ curves have been positioned for coincidence of their maxima. The $U'*U$ curve is shifted in energy with respect to the dN/dE curve by ~1 eV from the relative position used for $N(E)$ and $U*U$.

That is, the local density of states observed in EEAES on a Ni(110)-$c(2\times2)$S surface has the same structural features as the local density of states that is observed in INS on a similar surface. Their difference can be interpreted as a matter of degree; that is, the same structural features characterize the two DOS functions but the relative peak amplitudes differ (part of this difference results from the truncation assumption as described later in this section). Therefore, it is instructive to compare the INS $U(\zeta)$ curve in Fig. 8 with the EEAES $N(E)$ curve in Fig. 7 and invoke the findings of the model calculations in Sec. III to effect this comparison.

Let the $U(\zeta)$ curve of Fig. 8 be represented simply as the sum of three broad peaks which will be labeled d, r_1, and r_2. They have approximate locations of $r_1 \sim 5$ eV, $d \sim 0.5$ eV, and $r_2 \sim 10$ eV, and relative peak heights that decrease in the same order. According to the model calculations, these three peaks will produce three peaks in $N(E)$ via their convolution squares at the positions

$$\begin{aligned} &U(r_1)*U(r_1)=R_{11} \text{ at 10 eV},\\ &U(d)*U(d)=D \text{ at 1 eV},\\ &U(r_2)*U(r_2)=R_{22} \text{ at 20 eV}, \end{aligned} \tag{6}$$

while their convolution products will produce peaks in $N(E)$ at

$$\begin{aligned} &U(r_1)*U(d)=R_1D \text{ at 5.5 eV},\\ &U(r_1)*U(r_2)=R_{12} \text{ at 15 eV},\\ &U(d)*U(r_2)=DR_2 \text{ at 10.5 eV}. \end{aligned} \tag{7}$$

Consequently $N(E)$ can be expected to consist of principal features occurring near 1, 5, 10, 15, and 20 eV. In this manner it may be reasonable to associate these convolution effects with the features labeled A, B, C, D, and E in Fig. 10 (and in that order). However, it can, at most, be said that a large part of the information in any one of these features arises from the corresponding convolution effects. There are also background effects and peak-width effects to be added to each of the convolution terms of Eqs. (6) and (7) to approximate the observed line shape.

In order to appreciate the role of peak-width effects consider the most predominant feature in $N(E)$, namely, the local maximum at $\eta = 9.5$ eV. The contributions of the DOS function to this particular element of the $N(E)$ spectrum is, from Eq. (2),

$$\tilde{N}(4.75)=\int_0^{4.75} N(4.75-\Delta)N(4.75+\Delta)\,d\Delta. \tag{8}$$

It is evident from Eq. (8) that almost the entire DOS function contributes to $\tilde{N}(4.75)$. The first term of the integrand spans most of the upper half of the r_1 peak, plus the d peak, and all of the intervening background. The second term within the integrand covers all of the remaining r_1 peak and some of the leading edge of the r_2 peak. Thus the results of Eqs. (6) and (7) reveal only a part of the significance of a given element of line shape.

Owing to the pronounced narrow peak at 9.5 eV in $N(E)$, the dN/dE curve is dominated by the derivative of this peak. However, the fine structure lying both to the high- and low-energy sides of this peak in dN/dE is no less significant. According to Fig. (10) the spectra appear to contain significant information in a range of up to 10 eV to the high-energy side and up to ~20 eV to the low-energy side of this main peak.

The comparison of these data from two spectroscopies also should be expected to display differences associated with the properties that characterize the spectroscopies. For example, the electrons that yield the sulfur spectrum in EEAES have an average energy of ~145 eV while the corresponding spectrum in INS derives from electrons having energies that are lower by a factor of 10 or more. Therefore it might be expected that these two groups of electrons could have originated at different depths within the selvedge and consequently reflect different averages of local densities of states. The strong correlation of the two spectra, in spite of this basic difference in the two spectroscopies, is indic-

ative that the surface region being analyzed is thin enough and sufficiently close to the free-space interface to cause no appreciable attenuation effects. Hence it is concluded that EEAES and INS are surface selective in similar fashions. On the other hand, attenuation effects may not be as different in the two spectroscopies as the difference in Auger-electron energies between them. This follows from the expectation that the electron mean free path may pass through a minimum at some intermediate energy.[31]

The lower relative intensity of the structure on the high-energy side of the $N(E)$ maximum in the AES spectrum (i.e., the peak labeled B in Fig. 10) is interpreted as due to either a larger r_1 peak or a smaller d peak than noted with INS. It is not obvious why these differences should occur. One plausible reason might be, as already explained, the possible difference in local density of states that could be sampled by the two techniques. However, if this were true, it would be natural to expect the higher-energy electrons of the EEAES to originate from a broader range of surface thickness and possibly to include sulfur atoms essentially in the bulk. They should be expected, therefore, to show more nearly bulk properties: a smaller r_1 peak and a relatively larger d peak as compared with the INS data (see Fig. 8). Another possible explanation of the difference is that the surfaces examined by the two independent techniques may have important differences, such as, the absolute sulfur coverage in the Ni(110)-$c(2\times2)$S structure. It should be noted that the $c(2\times2)$S structure was produced by different techniques: In this work the nickel specimen was simply heated to produce the sulfur surface structure (presumably by diffusion of sulfur from the bulk).[25] Whereas in the INS work H_2S was dissociated on the specimen surface.[3(a)]

Differences in sulfur coverage between the experiment that generated the EEAES data and the one yielding the INS data were probably not too great and may even be too small to be detected except by a comparison such as presented here. The reason is evident in the difference between the $N(E)$ and $U*U$ curves in Fig. 10 in the region between B and C. Effects due to the INS limit ζ_{max} are not yet present in this region of the $U*U$ curve. Thus we can consider the significance of the difference in magnitudes of the curves if it is all attributed to dissimilar sulfur coverage. First, note that in Fig. 10 the difference between $N(E)$ and $U*U$ at C is slightly exaggerated because the curves are not superimposed at C. The remaining difference in magnitude between the curves cannot be considered to be a large effect when it is noted that these curves are the convolution of DOS functions in which small changes in DOS peak height, peak width, or background result in significant alterations in the final convolution.

The difference in magnitude between $N(E)$ and $U*U$ in the region $11 \leq \eta \leq 22$ and the correlation of peaks E and e (see Fig. 10) in this region are related to the U-truncation assumption. The more rapid falloff of the calculated $U*U$ relative to $N(E)$ is due in part to this assumption. That is, by forcing U to be zero in a region where it may be finite produces a smaller magnitude fold function in the range of the fold affected by the truncation. This diminution effect is greatest at $\eta = 22$ eV and least at $\eta = 11$ eV. On the other hand, the correlation of peaks E and e at the same energy is evidence that the truncation assumption has not eradicated all meaningful information in this range, a consequence of the natural redundancy inherent in convolution integrals and evidence that the truncation assumption is not too far from reality.

VII. CONCLUSIONS

It has been shown that electron-excited Auger-electron spectra correlate with ion-neutralization spectra for the Ni(110)-$c(2\times2)$S surface. The correlation was demonstrated with respect to fine-structure features in dN/dE curves of EEAES and truncated, folded, and differentiated transition-probability spectra of INS. This correlation is empirical evidence that both spectroscopies are surface selective in similar fashions.[32]

This experiment demonstrates a considerable gain in useful information from AES by the expedient removal of the secondary-electron-cascade background so that a direct analysis of $N(E)$ data obtains.

The onset of the Auger line belonging to an $L_{2,3}VV$ transition between the sulfur core state and Ni(110)-$c(2\times2)$S band states and to an M_1VV transition between a nickel core state and the band have been demonstrated by characteristic thresholds. The agreement of the position of the thresholds with tabulated binding energies suggests the usefulness of thresholds as a distinguishing characteristic of iVV-type transitions.

It has been shown that for the particular set of INS $U(\zeta)$ data used here it is possible to set $U(\zeta) = 0$ for $\zeta > \zeta_m$, the natural cutoff of the INS data, and then to fold the truncated function to recover some information about the fold in the range $\zeta > \zeta_m$. In general, this procedure should be applicable whenever the content of the truncated region of the unfold is small compared with the content of the fold function in the redundant region affected by the truncated range of $U(\zeta)$.

Finally, it is noted that the Auger-fine-structure analysis reported here has been effected without recourse to secondary mechanisms such as characteristic energy losses, other Auger transitions,

or characteristic energy gains.

ACKNOWLEDGMENTS

The author wishes to express his gratitude to D. Romano and H. Cunningham for technical assistance in this research. Helpful discussions of the work were provided by Dr. F. Steinrisser and by Dr. W. Winterbottom and Dr. C. Davis. The latter two also assisted with a critical reading of the manuscript.

The author is grateful to Dr. Hagstrum for suggesting improvements to the manuscript and for discussion leading to the comments appended to Sec. VI. Unpublished fold data $F(\zeta)$, by Dr. Becker and Dr. Hagstrum for the Ni(110)-$c(2\times2)$S surface, were kindly provided and used to compare $U*U$ and $F(\zeta)$ as discussed in Sec. VI.

The author is also indebted to Dr. C. J. Powell for a critical reading of the manuscript and for ameliorative recommendations.

APPENDIX

The method of calculating Auger line shapes from models for the transition density function is summarized in this appendix.

A transition density function $u(\zeta)$ is composed of a background function $b(\zeta)$ and a set of peaked functions $p_i(\zeta)$. It is in effect "turned on" at the Fermi level $\zeta=0$ and "turned off" at the band edge $\zeta=\zeta_b$ by the convenience of a rectangular function $\Pi(\zeta)$ which is the sum of two Heaviside unit step functions $H(\zeta,\zeta_b)$:

$$\Pi\left(\frac{\zeta}{\zeta_b}\right)=H\left(\frac{\zeta}{\zeta_b}\right)-H\left(\frac{\zeta-\zeta_b}{\zeta_b}\right), \tag{A1}$$

where $H(X)=0$ if $X\le 0$ and $H(X)=1$ if $X>0$. As a result of this definition,

$$\Pi\left(\frac{\zeta}{\zeta_b}\right)=\begin{cases}0, & \zeta\le 0\\ 1, & 0<\zeta<\zeta_b\\ 0, & \zeta_b\le\zeta\ .\end{cases} \tag{A2}$$

Thus in the integrals to follow $u(\zeta)$ is represented in the following manner, e.g.,

$$u_j(\zeta)=\Pi\left(\frac{\zeta}{\zeta_b}\right)u(\zeta)=\Pi\left(\frac{\zeta}{\zeta_b}\right)\left[b(\zeta)+\sum_i p_i(\zeta)\right],\quad j=1,2. \tag{A3}$$

The Auger line shape is related to $u(\zeta)$ through the following symmetric convolution integral:

$$\begin{aligned}\tilde{u}_{12}=u_1*u_2=&\Pi\left(\frac{2\zeta}{\zeta_b}\right)\int_0^{\zeta}\Pi\left(\frac{\zeta+\Delta}{\zeta_b}\right)u_1(\zeta+\Delta)\\ &\times\Pi\left(\frac{\zeta-\Delta}{\zeta_b}\right)u_2(\zeta-\Delta)\,d\Delta+\Pi\left(\frac{2\zeta_b-2\zeta}{\zeta_b}\right)\int_0^{\zeta_b-\zeta}\Pi\left(\frac{\zeta+\Delta}{\zeta_b}\right)\\ &\times u_1(\zeta+\Delta)\,\Pi\left(\frac{\zeta-\Delta}{\zeta_b}\right)u_2(\zeta-\Delta)\,d\Delta\ .\end{aligned} \tag{A4}$$

The first integral applies to ζ in the upper half of the band, $0\le\zeta\le\zeta_b/2$, while the second integral applies to ζ in the lower half of the band, $\zeta_b/2\le\zeta\le\zeta_b$. Subscripts 1 and 2 on ζ indicate that the transition density function for the up electron in the two-electron Auger transition process may differ from that for the down electron. Either of the two electrons may originate at the levels $\zeta+\Delta$ or $\zeta-\Delta$. Consequently there is an inherent degeneracy factor in Eq. (A4) which is equal to two. The energy distribution $N(E)$ of Auger electrons external to a specimen is assumed to be related to Eq. (A4) according to

$$N(E)\propto P(E)\tilde{u}_{12}(E)\ , \tag{A5}$$

where $P(E)$ is the escape probability for internal electrons encountering the surface. Equation (A5) must also be folded with a characteristic instrument function in order to relate (A5) to an experimentally observed Auger line shape. Consideration of Auger line shape will be limited here to an analysis of $\tilde{u}_{12}$.

The asymmetric form of the convolution integral is obtained from Eq. (A4) by the transformations

$$\xi=\zeta+\Delta\quad\text{and}\quad\eta=2\zeta \tag{A6}$$

which yield

$$\begin{aligned}\tilde{u}_{21}(\eta)=&\Pi\left(\frac{\eta}{\zeta_b}\right)\int_0^{\eta}u_1(\xi)u_2(\eta-\xi)\,d\xi\\ &+\Pi\left(\frac{2\zeta_b-\eta}{\zeta_b}\right)\int_{\eta-\zeta_b}^{\zeta_b}u_1(\xi)u_2(\eta-\xi)\,d\xi\ .\end{aligned} \tag{A7}$$

Equation (A7) is the integral of the fold of u_2 upon u_1 at $\xi=\zeta$. Note the change in limits of integration that is introduced upon simplification of the Π functions. Use of the property that $\tilde{u}_{12}=\tilde{u}_{21}$ provides a convenient check on results obtained from Eq. (A7).

Insertion of Eq. (A3) into Eq. (A7) for u_1 and u_2 produces a sum of convolution products of the type b_1*b_2, b_i*p_j, and p_i*p_j $(i,j=1,2)$. Thus further examination of the properties of Eq. (A7) will be concentrated upon the individual convolution products of the functions that make up u_i in Eq. (A3). These results can then be added to obtain a particular representation of Eq. (A7) for a specific form of Eq. (A3).

Let $u(\xi)$ be made up of a background function $b(\xi)$, which may be zero, a constant, or linear in ξ, and two normalized Gaussian functions p_a and p_b centered at $\xi=a$ and $\xi=b$ having widths $\alpha/\sqrt{2}$ and $\beta/\sqrt{2}$, respectively:

$$u(\xi)=b(\xi)+p_a(\xi)+p_b(\xi)\ , \tag{A8}$$

where

$$b(\xi)=\begin{cases}0\\ a\\ a+b\xi\end{cases} \tag{A9}$$

and

$$p_a = (A/\sqrt{\pi\alpha})\, e^{-[(\xi-a)/\alpha]^2} \tag{A10}$$

(similarly for p_b), where p_a/A is normalized and therefore A serves as an adjustable amplitude parameter which is always equal to the area under the Gaussian p_a.

The use of Eq. (A8) to model a transition density function will lead to an Auger line shape through Eq. (A7) that will be composed of various convolution products as summarized in what follows (recall that $\eta = 2\xi$, and $0 \le \eta \le 2\xi_b$).

(I) $u_1 = a$, $u_2 = b$:

$$\tilde{u}_{12}(\eta) = ab\left[\eta\,\Pi\left(\frac{\eta}{\xi_b}\right) + (2\xi_b - \eta)\Pi\left(\frac{2\xi_b - \eta}{\xi_b}\right)\right], \tag{A11}$$

which is an isosceles triangle peaked at the center of the band $\eta = \xi_b$, with peak height $ab\xi_b$ and area $\frac{1}{2}ab\xi_b^2$ [see example in Figs. 3(b) and 4(a), where $a = b$].

$$\tilde{u}'_{12}(\eta) = ab\left[\Pi\left(\frac{\eta}{\xi_b}\right) - \Pi\left(\frac{2\xi_b - \eta}{\xi_b}\right)\right], \tag{A12}$$

which is a step of height ab symmetric about the abscissa and positioned at the center of the band.

(II) $u_1 = a$, $u_2 = b\xi$:

$$\tilde{u}_{12}(\eta) = \tfrac{1}{2}ab\left[\eta^2\Pi\left(\frac{\eta}{\xi_b}\right) + (2\xi_b\eta - \eta^2)\Pi\left(\frac{2\xi_b - \eta}{\xi_b}\right)\right]. \tag{A13}$$

$\tilde{u}_{12}$ is parabolic in nature (two parabolic sections matched at $\eta = \xi$ with a discontinuous derivative) with a maximum at the band center $\eta = \xi_b$. It has a maximum amplitude of $2ab\xi_b^2$ and an area $2ab\xi_b^3$.

$$\tilde{u}'_{12}(\eta) = ab\left[\eta\Pi\left(\frac{\eta}{\xi_b}\right) + (\xi_b - \eta)\Pi\left(\frac{2\xi_b - \eta}{\xi_b}\right)\right]. \tag{A14}$$

(III) $u_1 = a\xi$, $u_2 = b\xi$:

$$\tilde{u}_{12}(\eta) = \tfrac{1}{6}ab\left[\eta^3\Pi\left(\frac{\eta}{\xi_b}\right) + (-\eta^3 + 6\eta\xi_b^2 - 4\xi_b^3)\Pi\left(\frac{2\xi_b - \eta}{\xi_b}\right)\right]. \tag{A15}$$

$\tilde{u}_{12}$ is cubic having a maximum located at $\eta = (\sqrt{2}+1)\xi_b$, having a magnitude $\frac{2}{3}(\sqrt{2}-1)ab\xi_b^3$, and an area $\frac{2}{3}ab\xi_b^4$ [see example in Fig. 4(b)].

$$\tilde{u}'_{12}(\eta) = \tfrac{1}{2}ab\left[\eta^2\Pi\left(\frac{\eta}{\xi_b}\right) + (-\eta^2 + 2\xi_b^2)\Pi\left(\frac{2\xi_b - \eta}{\xi_b}\right)\right]. \tag{A16}$$

The derivative $\tilde{u}'_{12}$ is continuous at the center of the band.

(IV) $u_1 = b$, $u_2 = (A/\sqrt{\pi\alpha})\, e^{-[(\xi-a)/\alpha]^2}$:

$$\tilde{u}_{12}(\eta) = Ab\left[G\left(\frac{\xi - a}{\alpha}\right)\Big|_0^{\eta}\Pi\left(\frac{\eta}{\xi_b}\right) + G\left(\frac{\xi - a}{\alpha}\right)\Big|_{\eta-\xi_b}^{\xi_b}\Pi\left(\frac{2\xi_b - \eta}{\xi_b}\right)\right], \tag{A17}$$

where $G\big|_0^{\eta}$ is a segment of a Gaussian step $G\big|_{-\infty}^{\infty}$ defined as

$$G\left(\frac{\xi - a}{\alpha}\right)\Big|_{\eta_1}^{\eta_2} = \frac{1}{\sqrt{\pi\alpha}}\int_{\eta_1}^{\eta_2} e^{-[(\xi-a)/\alpha]^2} d\xi\,. \tag{A18}$$

Eq. (A17) can be reduced to a single term,

$$\tilde{u}_{12}(\eta) = AbG\left(\frac{\xi - a}{\alpha}\right)\Big|_0^{\eta}\Pi\left(\frac{\eta}{2\xi_b}\right), \tag{A19}$$

which can also be expressed as

$$\tilde{u}_{12}(\eta) = \tfrac{1}{2}Ab\left\{\mathrm{erf}\left[\frac{\sqrt{\pi}}{\alpha}(\eta - a)\right] + \mathrm{erf}\left(\sqrt{\pi}\,\frac{a}{\alpha}\right)\right\}. \tag{A20}$$

If the Gaussian is sufficiently narrow so as to be removed from the boundaries $\xi = 0$ (and $\xi = \xi_b$) by several half-widths [see example in Fig. 5(b)] then the full Gaussian step will be present within the boundaries and will be positioned at $\eta = a$ [i.e., the position of its maximum slope is halfway between the threshold of $\tilde{u}_{12}$ and the maximum in the convolution square of the Gaussian peak; see (VI)]. The maximum step height is Ab. The derivative of $\tilde{u}_{12}$ is given by

$$\tilde{u}'_{12}(\eta) = \frac{Ab}{\sqrt{\pi\alpha}}\, e^{-[(\eta-a)/\alpha]^2}\Pi\left(\frac{\eta}{2\xi_b}\right), \tag{A21}$$

which is a normalized Gaussian centered at $\eta = a$ and multiplied by a constant Ab.

(V) $u_1 = b\xi$, $u_2 = (A/\sqrt{\pi\alpha})\, e^{-[(\xi-a)/\alpha]^2}$:

$$\tilde{u}_{12}(\eta) = Ab(\eta - a)\,G\left(\frac{\xi - a}{\alpha}\right)\Big|_0^{\eta/2}\Pi\left(\frac{\eta}{2\xi_b}\right) + \frac{Ab\alpha}{2/\pi}\left\{\left(e^{-[(\eta-a)/\alpha]^2} - e^{-(a/\alpha)^2}\right)\Pi\left(\frac{\eta}{\xi_b}\right) + \left(e^{-[(\xi_b-a)/\alpha]^2} - e^{-[(\eta-\xi_b-a)/\alpha]^2}\right)\Pi\left(\frac{2\xi_b - \eta}{\xi_b}\right)\right\}. \tag{A22}$$

The convolution of a linear background with a Gaussian peak produces a complex function that can be expressed in three parts as given by Eq. (A22). The first term is the product of a linear function $(\eta - a)$ with a Gaussian step and spans the complete band. The next term is a Gaussian peak, minus a constant, centered at $\eta = a$ in the upper half of the band. The third term, in the lower half of the band, is the difference between a constant and a Gaussian centered at $\eta = \xi_b + a$, which results in an inverted Gaussian centered at $\eta = \xi_b + a$. The second and third terms vanish at the boundaries $\eta = 0$ and $\eta = 2\xi_b$, respectively.

The derivative of $\tilde{u}_{12}$ is given by

$$\tilde{u}'_{12}(\eta) = Ab\left[\left(\frac{\eta - a}{\sqrt{\pi\alpha}}\right)e^{-[(\eta-a)/\alpha]^2} + G\left(\frac{\xi - a}{\alpha}\right)\Big|_0^{\eta}\right]\Pi\left(\frac{\eta}{2\xi_b}\right) - \frac{Ab}{\sqrt{\pi}}\left[\left(\frac{\eta - a}{\alpha}\right)e^{-[(\eta-a)/\alpha]^2}\Pi\left(\frac{\eta}{\xi_b}\right) + \left(\frac{\eta - \xi_b - a}{\alpha}\right)e^{-[(\eta-\xi_b-a)/\alpha]^2}\Pi\left(\frac{2\xi_b - \eta}{\xi_b}\right)\right], \tag{A23}$$

which consists of two Gaussian derivatives centered at $\eta = a$ and $\eta = \xi_b + a$ plus a Gaussian step at $\eta = 2a$.

(VI) $u_1 = (A/\sqrt{\pi}\alpha)\, e^{-[(\xi-a)/\alpha]^2}$, $u_2 = (\beta/\sqrt{\pi}\alpha)\, e^{-[(\xi-b)/\beta]^2}$:

$$\tilde{u}_{12}(\eta) = \frac{AB}{[\pi(\alpha^2+\beta^2)]^{1/2}}\, e^{-(\eta-a-b)^2/(\alpha^2+\beta^2)} \times G\left[\frac{(\alpha^2+\beta^2)\,\xi - \alpha^2\eta - \alpha\beta^2 + b\alpha^2}{\alpha\beta(\alpha^2+\beta^2)^{1/2}}\right]_0^{\eta} \Pi\left(\frac{\eta}{2\xi_b}\right). \quad \text{(A24)}$$

$\tilde{u}_{12}(\eta)$ is a Gaussian centered at $\eta = a + b$ (the arithmetic mean of $\xi = a$ and $\xi = b$) with width $[(\alpha^2+\beta^2)/2]^{1/2}$ multiplied by a Gaussian step. In the case $\alpha = \beta$, i.e., the two Gaussians u_1 and u_2 have equal widths, their convolution product becomes

$$\tilde{u}_{12}(\eta)\Big|_{\alpha=\beta} = \frac{AB}{\alpha(2\pi)^{1/2}}\, e^{-(\eta-a-b)^2/2\alpha^2} \times G\left[\frac{2\xi - \eta - a + b}{\alpha\sqrt{2}}\right]_0^{\eta} \Pi\left(\frac{\eta}{2\xi_b}\right), \quad \text{(A25)}$$

which is composed of a Gaussian, whose width is $\sqrt{2}$ larger than u_1 or u_2, multiplied by a Gaussian step [see example in Fig. 3(a)].

[1] L. A. Harris, J. Appl. Phys. **39**, 1419 (1968); J. Appl. Phys. **39**, 1428 (1968); R. E. Weber and W. T. Peria, J. Appl. Phys. **38**, 4355 (1967); P. W. Palmberg, J. Appl. Phys. **38**, 2137 (1967); L. N. Tharp and E. J. Scheibner, J. Appl. Phys. **38**, 3320 (1967). See, also the bibliography on AES by D. T. Hawkins, Bell Telephone Laboratories, No. 201, March 1972 (unpublished); the bibliography on AES by T. W. Haas, G. J. Dooley, J. T. Grant, A. G. Jackson, and M. P. Hooker, *Progress in Surface Science* (Pergamon, New York, 1971), Vol. 12; and the review article on LEED and AES by E. N. Sickafus and H. P. Bonzel, in *Progress in Surface and Membrane Science*, edited by J. F. Danielli, M. D. Rosenberg, and D. A. Cadenhead (Academic, New York, 1971), Vol. 4.

[2] J. J. Lander, Phys. Rev. **91**, 1382 (1953).

[3] See, for example, H. D. Hagstrum, Phys. Rev. **150**, 495 (1966); H. D. Hagstrum and G. E. Becker, (a) J. Chem. Phys. **54**, 1015 (1971); (b)Phys. Rev. **159**, 572 (1967).

[4] G. F. Amelio and E. J. Scheibner, Surf. Sci. **11**, 242 (1968).

[5] R. G. Musket and R. J. Fortner, Phys. Rev. Lett. **26**, 80 (1971).

[6] E. J. LeJeune, Jr. and R. D. Dixon, J. Appl. Phys. **43**, 1998 (1972).

[7] G. F. Amelio, Surf. Sci. **22**, 301 (1970).

[8] G. E. Becker and H. D. Hagstrum, Surf. Sci. **30**, 125 (1972). The author is grateful to Dr. Becker and Dr. Hagstrum for supplying the work-function value and the transition density curves prior to their publication.

[9] M. Pessa, S. Aksela, and M. Karras, Phys. Lett. A **31**, 382 (1970).

[10] H. Slätis and M. Rockberger, Ark. Fys. **40**, 49 (1968).

[11] Y. Y. Liu and R. G. Albridge, Nucl. Phys. A. **92**, 139 (1967).

[12] T. W. Haas, J. T. Grant, and G. J. Dooley, III, Phys. Rev. B **1**, 1449 (1970).

[13] N. J. Taylor, Surf. Sci. **15**, 169 (1969).

[14] W. M. Mularie and T. W. Rusch, Surf. Sci. **19**, 469 (1970).

[15] L. H. Jenkins and M. F. Chung, Surf. Sci. **26**, 151 (1971).

[16] W. M. Mularie and W. T. Peria, Surf. Sci. **26**, 125 (1971).

[17] M. Suleman and E. B. Pattinson, J. Phys. F **1**, L21 (1971).

[18] H. D. McGuire and P. D. Augustus, J. Phys. C **4**, L174 (1971).

[19] J. A. D. Matthew and C. M. K. Watts, Phys. Lett. A **37**, 239 (1971).

[20] C. C. Chang, Surf. Sci. **23**, 283 (1970).

[21] T. W. Haas, J. T. Grant, and G. J. Dooley, III, J. Appl. Phys. **43**, 1853 (1972).

[22] R. J. Fortner and R. G. Musket, Surf. Sci. **28**, 339 (1971).

[23] J. P. Coad and J. C. Riviere, Phys. Lett. A **35**, 185 (1971).

[24] H. D. Hagstrum and G. E. Becker, Phys. Rev. B **4**, 4187 (1971). Their nomenclature is used in the present paper.

[25] E. N. Sickafus, Surf. Sci. **19**, 181 (1970).

[26] E. N. Sickafus, Rev. Sci. Instrum. **42**, 933 (1971).

[27] Characteristic-electron-energy-loss measurements were made in this system in collaboration with F. Steinrisser, E. N. Sickafus, and F. Steinrisser, Phys. Rev. B **6**, 3714 (1972).

[28] See, for example, binding energies relative to the Fermi level as tabulated by J. A. Bearden and A. F. Burr [Rev. Mod. Phys. **39**, 125 (1967)]. The use in Eq. (3) of binding energies E' relative to the Fermi level has the effect of reducing the coefficient of ϕ by a factor of 2 obtaining $E = |E_i| - 2\zeta - \phi$.

[29] J. G. Hanus, MIT Solid State and Molecular Theory Group Quarterly Report No. 44, 1962 (unpublished).

[30] F. Steinrisser and E. N. Sickafus, Phys. Rev. Lett. **27**, 992 (1971).

[31] J. J. Quinn, Phys. Rev. **126**, 1435 (1962).

[32] In view of the correlation that has been demonstrated between Auger-electron spectroscopy and ion-neutralization spectroscopy a new emphasis may be useful in their abbreviations. They are both Auger-electron spectroscopies. However, it has become customary to use AES to refer to the electron-excitation spectroscopy and INS to refer to the ion-neutralization spectroscopy. A more useful abbreviation, by virtue of the clear reference to their distinguishing characteristics, would be EEAES and INAES.